AGU PUBLICATIONS

JGR

Journal of Geophysical Research: Oceans

RESEARCH ARTICLE

10.1002/2016JC012603

Key Points:
- The Ob-dominated waters of the Ob-Yenisei river plume can isolate the Yenisei discharge from mixing with ambient sea water
- The isolation process induces northward transport of the low-saline and warm Yenisei-dominated waters
- The "isolation" configuration is estimated to form regularly in August-October and depend on wind forcing and river discharge conditions

Correspondence to:
A. A. Osadchiev,
osadchiev@ocean.ru

Citation:
Osadchiev, A. A., A. S. Izhitskiy, P. O. Zavialov, V. V. Kremenetskiy, A. A. Polukhin, V. V. Pelevin, and Z. M. Toktamysova (2017), Structure of the buoyant plume formed by Ob and Yenisei river discharge in the southern part of the Kara Sea during summer and autumn, *J. Geophys. Res. Oceans*, *122*, doi:10.1002/2016JC012603.

Received 30 NOV 2016
Accepted 26 JUN 2017
Accepted article online 5 JUL 2017

Structure of the buoyant plume formed by Ob and Yenisei river discharge in the southern part of the Kara Sea during summer and autumn

A. A. Osadchiev[1], A. S. Izhitskiy[1], P. O. Zavialov[1], V. V. Kremenetskiy[1], A. A. Polukhin[1], V. V. Pelevin[1], and Z. M. Toktamysova[2]

[1]Shirshov Institute of Oceanology, Russian Academy of Sciences, Moscow, Russia, [2]Higher School of Economics, Moscow, Russia

Abstract This article focuses on the interaction between the Ob- and Yenisei-dominated parts of the large Ob-Yenisei buoyant plume formed in the southern part of the Kara Sea during ice-free periods. It was shown that certain wind forcing and river discharge conditions cause the formation of a specific structure of the Ob-Yenisei plume with significantly different properties of the Ob- and Yenisei-dominated water masses. Under these conditions, the Yenisei runoff generates a narrow coastal current propagating northward from the Yenisei Gulf along the Taymyr Peninsula, which is isolated by the Ob-dominated water mass from ambient sea water. As a result, the low-salinity Yenisei-dominated water mass occupies a relatively small area, while more saline Ob-dominated water mass spreads over a wide area between the Gulf of Ob and the Taymyr Peninsula. The formation of the "isolation" configuration of the Ob-Yenisei plume described above is presumed to be caused by the eastward Ekman transport and the resulting downwelling flow of the Ob-dominated waters under the low-saline and warm Yenisei-dominated waters along the Taymyr Peninsula. Based on satellite imagery, wind reanalysis, and river discharge data collected and derived for the period of 2005–2011, it was estimated that the "isolation" configuration is regularly formed during late summer and autumn when the Ob discharge to the Kara Sea exceeds the Yenisei discharge and the local atmospheric circulation is dominated by the northerly wind regime. Assessment of the frequency and duration of the occurrence of the "isolation" configuration showed their synoptic time scale and significant interannual variability.

Plain Language Summary This study focuses on spreading of discharge of the Ob and Yenisei rivers in the Kara Sea. Under certain wind and discharge conditions the Ob discharge isolates the Yenisei discharge from the ambient sea and induces northward transport of low-saline Yenisei-dominated water to the open part of the Kara Sea. This transport is presumed to regularly occur in summer and late autumn and can influence ice formation processes in the central part of the Kara Sea. Spreading of the low-saline Yenisei-dominated water can also affect primary productivity and food webs in the study region.

1. Introduction

The Kara Sea is a shallow semienclosed sea in the Arctic Ocean located between the northern coast of Siberia, Novaya Zemlya, Severnaya Zemlya, and Taymyr Peninsula (Figure 1). It is connected with the Barents (to the west) and Laptev (to the east) seas through the narrow Kara and Vilkitsky straits. In the north, the Kara Sea is open to the Barents Sea and the deep basin of the Arctic Ocean. The sea depth generally does not exceed 50 m at the southern and southwestern parts of the Kara Sea, which is approximately 40% of its area.

Freshwater discharge significantly modulates climatology of the Arctic; in particular, it affects ocean stratification, heat flux, circulation, biogeochemical cycling, ice cover, and deep water formation [e.g., *Carmack et al.*, 2016; *Nummelin et al.*, 2016]. The Kara Sea receives approximately 1350 km^3 of river water annually, which is more than a quarter of the total continental runoff to the Arctic Ocean [*Pavlov and Pfirman*, 1995; *Gordeev and Tsirkunov*, 1998]. Most of this volume is discharged from the Yenisei Gulf (630 km^3 yr^{-1} from the Yenisei River) and the Gulf of Ob (400 km^3 yr^{-1} from the Ob River and more than 85 km^3 yr^{-1} from the Taz, Pur, and other small rivers) (Figure 1).

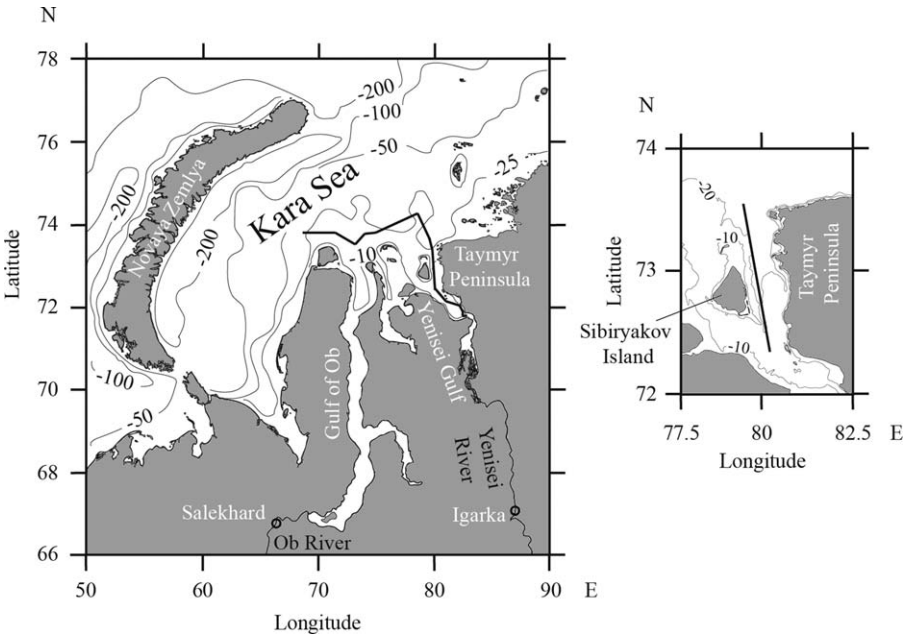

Figure 1. Bathymetry of the study region (in m), gauge stations at the Ob and Yenisei rivers (circles), and the ship track (black line) of the field survey performed on 16–18 September 2011 at the southern part of the Kara Sea (left); location of the Yenisei section between the Taymyr Peninsula and the Sibiryakov Island (right).

The hydrological regime of Yenisei, Ob, and other rivers that enter the Kara Sea is characterized by a low discharge rate during cold season (October–May) and a flooding period during summer and early autumn [*Pavlov and Pfirman*, 1995]. In particular, more than 70% of the annual continental runoff into the Kara Sea is discharged from the Ob and Yenisei gulfs from June to September, which is approximately 3% of the total annual continental runoff into the world ocean [*Meade et al*., 2000; *Oki and Kanae*, 2006]. This huge volume of fresh water forms a large buoyant plume that occupies an area of up to 350,000 km^2 in the southern part of the Kara Sea [*Johnson et al*., 1997; *Zavialov et al*., 2015].

The general circulation at the Kara Sea is governed by water exchange with the Barents Sea, deep basin of the Arctic Ocean, and river runoff. Surface waters at the southern part of the Kara Sea freshened by the Ob and Yenisei discharge are transported mainly northeast along the Siberian coast and north to the Novaya Zemlya and open Arctic Ocean [*Pavlov and Pfirman*, 1995; *Harms and Karcher*, 1999; *McClimans et al*., 2000; *Panteleev et al*., 2007]. However, the surface circulation in the southern part of the Kara Sea occupied by the Ob-Yenisei river plume strongly depends on wind forcing conditions and is characterized by high spatial and temporal variability [*Zatsepin et al*., 2010, 2015]. M2 is the main tidal constituent in the southern part of the Kara Sea, with its amplitude estimated as 0.2–0.5 m. Velocities of tidal currents in the study area do not exceed 0.2 m s^{-1}; therefore, tidal mixing has limited influence on the Ob-Yenisei river plume [*Kagan et al*., 2010, 2011].

The Kara Sea is frozen during the majority of a year. The southern part of the sea adjacent to the Ob and Yenisei gulfs is covered by landfast ice (~1.8 m thick) from November to June. The ice regime in this area is significantly influenced by continental runoff [*Dmitrenko et al*., 2000]. The summer freshet discharge of relatively warm water from the Ob and Yenisei rivers accelerates breaking of the landast ice and transport of ice floes to the central part of the Kara Sea. As a result, during late summer and autumn, the share of remnant ice water in the surface layer is negligible in the southern and central parts of the Kara Sea [*Dubinina et al*., 2017].

Many previous studies focused on the important role of the Ob-Yenisei river plume in the large-scale physical, chemical, and biological processes in the Kara Sea [*Neelov and Kouraev*, 1996; *Harms and Karcher*, 1999; *McClimans et al*., 2000; *Harms and Karcher*, 2005; *Galimov et al*., 2006; *Panteleev et al*., 2007; *Zatsepin et al*., 2010; *Makkaveev et al*., 2015; *Zavialov et al*., 2015; *Zatsepin et al*., 2015]. Other papers examined the chemical and biological characteristics of the plume and spatial and temporal variations in these parameters [*Gordeev et al*., 1996; *Köhler et al*., 2003; *Gebhardt et al*., 2004; *Unger et al*., 2005; *Makkaveev et al*., 2010; *Kubryakov*

et al., 2016]. However, little attention has been paid to the physical aspects of plume evolution that results from the interaction between the Yenisei and Ob outflows (hereinafter, including all river waters discharged into the Gulf of Ob), and the ambient sea under various external forcing conditions.

An essential feature of the Ob-Yenisei plume is a significant spatial heterogeneity of the physical and chemical characteristics of its far-field part, caused by the following reasons. First, although the Ob and Yenisei gulfs are adjacent to one another, they are distinctly separated and the distance between them (~250 km) is significantly greater than the local Rossby deformation radius (~5 km). As a result, the Ob and Yenisei discharges dominate plume areas adjacent to the respective gulfs and form complex mixing zones within the plume. This situation differs from buoyant plumes formed by two or more rivers sharing the same estuary (e.g., the Parana and Uruguay rivers) or joint delta (e.g., the Ganges and Brahmaputra rivers). Second, the different soil characteristics of the catchment areas of the Gulf of Ob (peatlands) and the Yenisei Gulf (permafrost) result in a significant difference between the physical and chemical properties of the Ob and Yenisei rivers [*Köhler et al*., 2003], which can be used to differentiate the Ob- and Yenisei-dominated parts of the plume. Finally, both freshwater sources have relatively equal discharge rates; therefore, spatial scales of the Ob- and Yenisei-dominated parts of the plume have the same order of magnitude and the internal structure of the far-field part of the Ob-Yenisei plume is significantly influenced by both rivers. There is only one other large and spatially nonuniform buoyant plume, formed from freshwater sources of which have properties similar to those of the Ob-Yenisei plume. This plume is formed in the northern part of the Andaman Sea by the Ayeyarwady River (13,000 $m^3\ s^{-1}$) and the Salween River (5000 $m^3\ s^{-1}$) that have deltas located 250 km apart [*Ramaswamy et al*., 2004; *Robinson et al*., 2007].

A number of observational, laboratory, and numerical modeling studies focused on the interaction between two or several river plumes and its influence on plume structure and dynamical characteristics under various river discharge configurations and external forcing conditions. They addressed geostrophic adjustment of river plumes [*Cenedese et al*., 2012], the diversity of plume frontal collision types [*Warrick and Farnsworth*, 2017], impact of river plume collisions on coastal circulation [*Burrage et al*., 2008; *Yuan et al*., 2011; *Mendes et al*., 2016], and transport pathways of river-borne material [*Osadchiev and Korshenko*, 2017]. However, we are not aware of any work that considers the formation of a buoyant plume from two large freshwater sources under external forcing conditions or any observational work that focuses on the related physical aspects of the internal structure of the Ob-Yenisei plume or the Ayeyarwady-Salween plume. Therefore, studying the Ob-Yenisei plume structure and the interaction between its water masses, which influence a large area of the Kara Sea, has certain societal and ecological significance.

In this study, we first identified the Ob-Yenisei plume water masses and the mixing zone formed between the plumes for the mid-September 2011 period. We did this using in situ data collected in the southern part of the Kara Sea and coincidental satellite imagery of ocean surface color. We show that the Yenisei-dominated water mass was isolated from the ambient sea by the Ob-dominated water mass during this period. Then, we analyzed the satellite images of the study region taken during ice-free periods during the summers and autumns of the period 2005–2011 and the related wind and river discharge data. These data sets reveal presumable roles of wind forcing and river discharge conditions in forming the "isolation" configuration of the Ob-Yenisei plume. Based on these data sets, we propose a dynamical setting for the "isolation" structure, which allows us to evaluate the seasonal and interannual variations in the frequency and duration of this structure.

The paper is organized as follows. Section 2 provides detailed information about the in situ data collected during field measurements in the southern part of the Kara Sea influenced by freshwater discharge in September 2011. Section 3 focuses on the identification of the different water types of the Ob-Yenisei plume based on the statistical analysis of the in situ data and its validation using vertical profiling data and satellite imagery. The analysis of the influence of external forcing on the structure of the Ob-Yenisei plume, the related dynamical interpretation, and the discussion about its variability are given in section 4, followed by the conclusions in section 5.

2. Data and Methods

2.1. Data Used

The in situ data used in this work was collected during the 59th cruise of the R/V "Academician Mstislav Keldysh." The field work addressed in this study took place in the southern part of the Kara Sea within the area influenced by the Ob and Yenisei discharges during 16–18 September 2011 (Figure 1).

Continuous measurements of temperature (T), salinity (S), and pH in the upper sea layer (1 m depth) were performed at 250 m spatial resolution along the ship track using a ship board pump-through system equipped by a CTD instrument (*SeaBird SBE911*) and by an ionometer (*Ekonis Expert 001*) with a glass composite pH electrode (*Akvilon*). Moreover, 28 water samples were collected from the pump-through cell mainly while crossing frontal zones and were used for the determination of total alkalinity (Alk) and pH in a vessel laboratory. Based on these samples as reference points, we reconstructed the continuous distribution of Alk using a partitioned correction calculated from the continuous data of T, S, and pH. Analyses of Alk were conducted using direct titration, i.e., the Bruyevich method with visual determination of the titration end point [*Edmond*, 1970; *DOE*, 1994; *Dickson et al*., 2003; *Pavlova et al*., 2008]. Accuracy of this method is equal to 2%, while its precision is 0.005 mg eqv/L.

Optical remote sensing was performed by a ship-mounted ultraviolet fluorescent LiDAR (UFL) and was used to derive simultaneous concentrations of chlorophyll a (Chl-a), total suspended matter (TSM), and colored dissolved organic matter (CDOM) at the sea surface with a 250 m spatial resolution along the ship track. The explicit description of the UFL instrument and the algorithms used for retrieving Chl-a, TSM, and CDOM are given in *Palmer et al*. [2013] and *Pelevin et al*. [2017].

Continuous vertical profiling measurements of T, S, and current velocity were performed using CTD (*Idronaut Ocean Seven 316*) and ADCP (*RDI WHM-300*) instruments along the Yenisei section located near the Taymyr Peninsula (Figure 1). The CTD and ADCP instruments were installed into a streamlined and dynamically balanced body, which was towed along the ship track aside of the ship wake and was repeatedly lowered and raised between the sea surface and the bottom. The horizontal towing velocity was about 2 m s^{-1}, while the vertical lowering/raising velocity was about 1 m s^{-1}. Horizontal/vertical resolution of the obtained CTD and ADCP data is about 0.5/0.25 m.

In addition to in situ data, we used surface distributions of Chl-a, TSM, and CDOM of the study region retrieved from MERIS/EnviSat satellite imagery taken in September 2011 with a 300 m spatial resolution. The Level 1 satellite products were processed using the MERIS Case-2 Regional water processing module [*Doerffer and Schiller*, 2008] of the BEAM software [*Fomferra and Brockmann*, 2015] based on neural network algorithms [*Doerffer and Schiller*, 1997].

Finally, to study the influence of external factors on the structure of the Ob-Yenisei plume, we used the following river runoff and wind forcing data. Discharge measurements at the Ob and Yenisei rivers were performed at gauge stations situated in the cities of Salekhard and Igarka, respectively (Figure 1). Although these stations are the most downstream stations for these rivers, the distances between Salekhard/Igarka and the mouths of the Ob/Yenisei gulfs are about 1000/800 km. Thus, by estimating the flow speed as 0.15 m s^{-1} in the Gulf of Ob [*Dianskii et al*., 2015], 0.3 m s^{-1} in the Yenisei Gulf [*Graevskii*, 1980; *Dolgopolova*, 2015], and 0.45 m s^{-1} in the Yenisei River [*Vakulovsky*, 2003; *Semizhon et al*., 2010], the hydrographs at the mouths of the Ob/Yenisei gulfs are presumed to be shifted forward by 87 and 35 days, respectively, compared to the hydrographs in Salekhard/Igarka.

The atmospheric influence on the Ob-Yenisei plume was examined using wind data obtained from a 12 h ERA-Interim reanalysis with a 0.75° resolution. The time series of the net surface Ekman transport at the study region for ice-free periods (July–October) were calculated in the following manner. First, the wind stress field τ was computed from the wind speed field $\boldsymbol{v}$ according to the equation $\tau = \rho_a C_D \boldsymbol{v}|\boldsymbol{v}|$, where ρ_a is the density of the air, C_D is the drag coefficient prescribed equal to 0.0013 [*Smith*, 1998]. Second, zonal and meridional components of the surface Ekman transport (M_x, M_y) were calculated as $M_x = \tau_y/f$, $M_y = -\tau_x/f$. Finally, the obtained values of the surface Ekman transport were averaged over the study area (72.5°N–74°N, 72.5°E–81°E) for a period of 3 days. This time scale was defined according to estimates of velocities of wind-driven currents and spatial scale of the study area given in *Kubryakov et al*. [2016].

2.2. Statistical Analysis of In Situ Data

The in situ measurements described above showed strong spatial heterogeneity of the far-field part of the Ob-Yenisei plume formed as a result of the interaction of the Ob and Yenisei discharges and the ambient sea water. The measurements demonstrated significant variability of the thermohaline, chemical, and optical water surface characteristics and revealed multiple frontal zones within the far-field part of the Ob-Yenisei plume. Comparison of measurements performed in the areas adjacent to the Ob and Yenisei gulfs,

i.e., strongly dominated by the Ob and Yenisei discharges, respectively, can be used to differentiate different water masses of the plume and identify their origins. Hereinafter, we will use the term "water mass" referring to real water body, while the term "water type" will represent the output of the applied statistical methods.

To identify the disposition of different water masses within the Ob-Yenisei plume, we applied a statistical analysis to the collected data sets of water surface characteristics (T, S, pH, Alk, Chl-a, TSM, and CDOM). The general scheme of the performed analysis is as follows. First, we identified statistically independent characteristics using the principal component analysis. Subsequently, we performed a cluster analysis of the independent variables. The resulting set of clusters along the ship track was interpreted as the disposition of different water masses of the Ob-Yenisei plume and was validated against satellite imagery and vertical CTD and ADCP profile data collected independently from the surface measurements. The detailed description of these operations is given below.

Clustering is the core procedure of the statistical analysis and aims to distinguish different water types within the Ob-Yenisei plume. Cluster analysis requires specific data preprocessing before its application to the in situ data. In particular, the input variables have to be statistically independent; otherwise, clustering will lead to inconsistent results. For this reason, we used multiple linear regressions to identify statistically independent variables among the seven registered sea surface characteristics. Salinity (S) was a priori considered as an independent variable, because it depends only on the concentration of the continental runoff in surface water and can be regarded as a passive tracer. According to *Dubinina et al*. [2017], we presume that the influence of other sources of fresh water, in particular, remnant ice melt, was negligible.

Statistical independence of the measured variables was examined as follows. Once a coefficient of determination between the considered variable and all other variables (including S) exceeded a certain threshold, the examined variable was regarded as dependent; otherwise, it was marked as statistically independent. The threshold value was prescribed equal to 0.8 as providing accurate and stable clustering results.

S, TSM, and pH were identified as statistically independent variables and defined three dimensions for the subsequent cluster analysis. The ship track was considered as a set of points in this three-dimensional space, and these points were separated into several groups using the k-means clustering algorithm with a prescribed number of clusters [*MacQueen*, 1967]. Values of S, TSM, and pH were initially adjusted to a common scale, i.e., normalized by their ranges, because we presume that all statistically independent variables have equal importance in distinguishing water types and should be weighted equally. Distances between points were calculated using standard Euclidean metrics. Initial centers of clusters were selected to maximize distances among them. The number of iterations was set to 50 to ensure stability of the clustering results.

The set of water types determined by cluster analysis represents different water masses of the Ob-Yenisei plume if the number of clusters is prescribed equal to the number of water masses. This number is initially unknown; therefore, the first cluster analysis was performed with ten prescribed clusters, which is a priori greater than the number of water masses. As a result, several water masses were distributed into more than one cluster, and this effect was indicated by significantly shorter distances between the centers of such clusters as compared to the distances between centers of other clusters. Based on this preliminary result, we identified five different water types of the Ob-Yenisei plume and performed the final cluster analysis with five prescribed clusters.

3. Structure of the Ob-Yenisei Plume

3.1. Water Types of the Ob-Yenisei River Plume

The resulting disposition of the clusters along the ship track is presented in Figure 2. We assume that different clusters represent different water masses of the Ob-Yenisei plume, formed as a result of interaction among the Ob and Yenisei runoffs and the ambient sea, due to the fact that the values of the analyzed variables were significantly different in these initial water masses.

First, we can identify that the region adjacent to the mouth of the Gulf of Ob (region I) is characterized by relatively simple configuration of water types as compared to the region adjacent to the Yenisei Gulf (region II). Region I consists of three clusters that occupy relatively long segments of the ship track (Figure 2). Average salinity values of the represented water types show direct coherence with their distances to the mouth

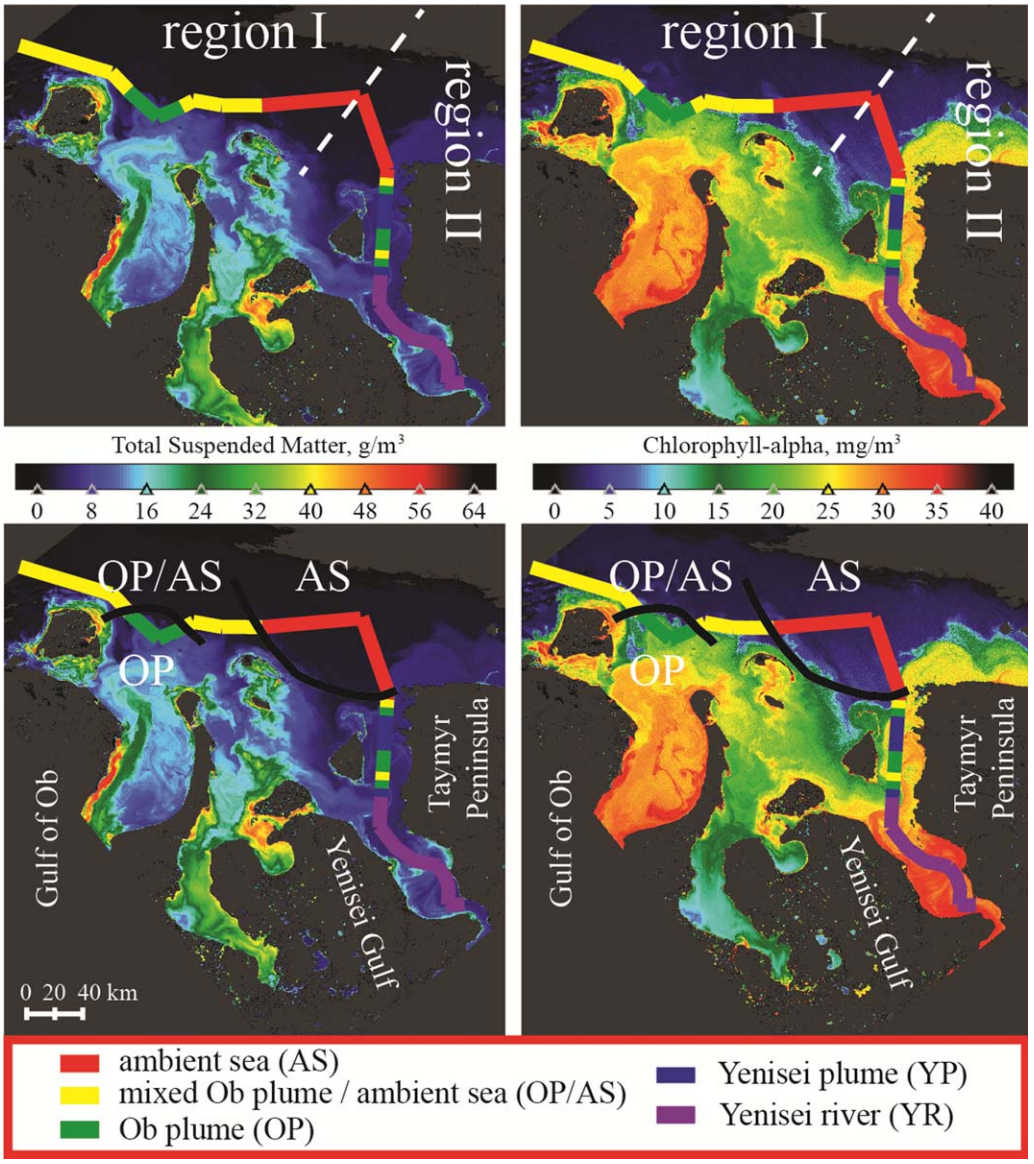

Figure 2. Satellite surface distributions of concentrations of total suspended matter (left) and chlorophyll-α (right) on 14 September 2011; disposition of the clusters along the survey track (top) and general configuration of water types at region I (bottom) of the Ob-Yenisei plume on 16–18 September 2011. Dashed white line illustrates regions I and II, solid black lines represent approximate disposition of frontal zones between the identified water types at region I.

of the Gulf of Ob. There was a steady salinity decrease from ~20 to the minimum value of 15 registered at the part of the ship track closest to the Gulf of Ob and then a steady increase to 28. More detailed information about the surface salinity distribution in the study region is given by *Zavialov et al*. [2015]. The disposition of water types in region I reproduces a typical configuration of a river plume; therefore, we can regard the most saline and distant water types from the Gulf of Ob cluster as "ambient sea water" (AS), the freshest and closest cluster as "Ob-dominated plume water" (OP), and a third cluster (OP/AS) that defines the mixing area between AS and OP.

Conversely, region II has a fragmentary configuration of five clusters, which occupy relatively short segments of the ship track (Figure 3). The average salinity values of clusters show dependence neither on their distance to the Yenisei Gulf nor to the Gulf of Ob. Nevertheless, the origins of the water masses represented by three of the five clusters appear to be from region I. The origins of the two remaining water masses also can be identified on the basis of their location and properties. The southernmost cluster, situated in the

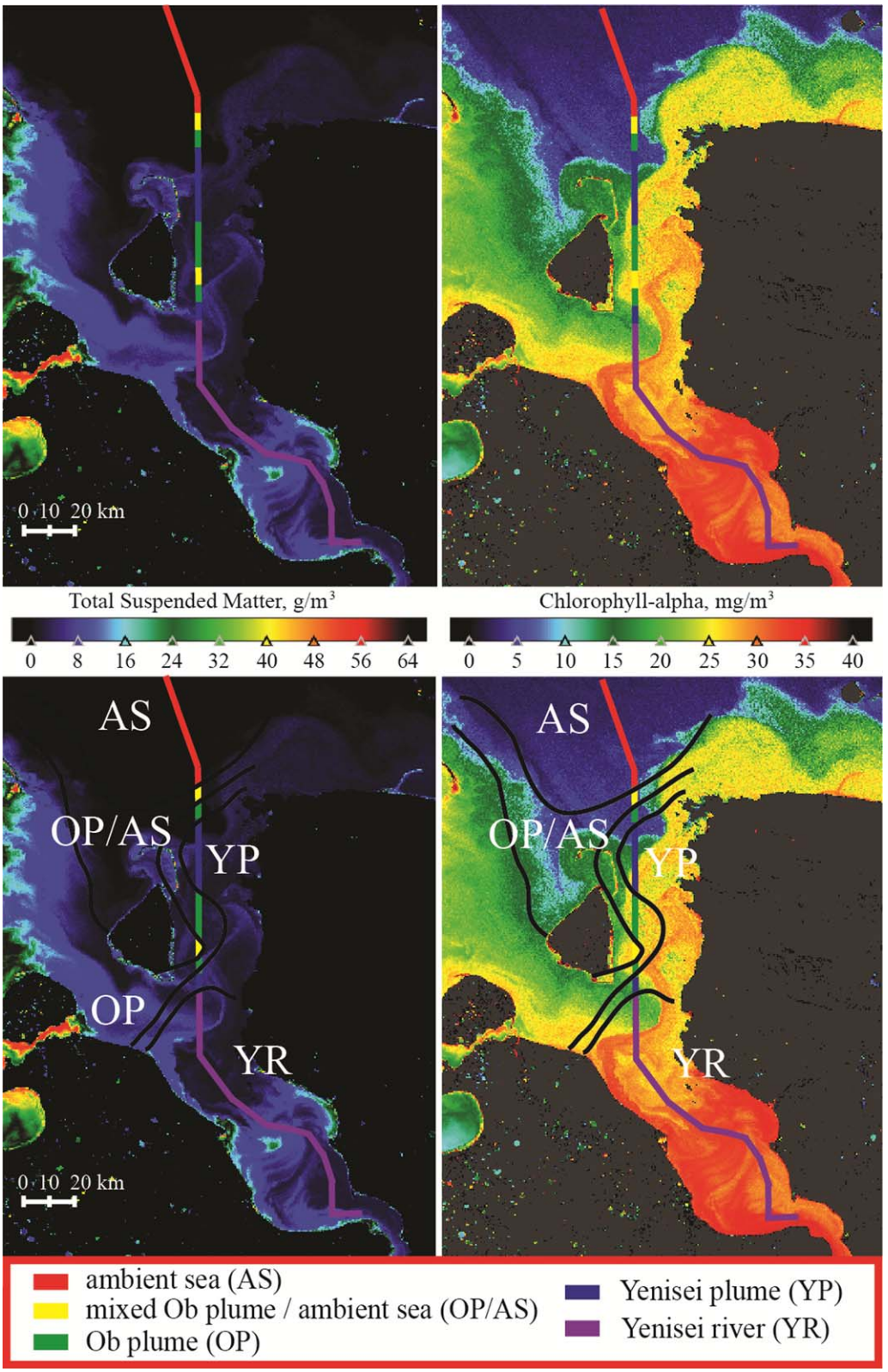

Figure 3. Satellite surface distributions of the total suspended matter (left) and chlorophyll-α (right) on 14 September 2011; disposition of the clusters along the survey track (top), and general configuration of water types (bottom) at region II on 16–18 September 2011. Solid black lines represent approximate disposition of frontal zones between the identified water types at region II.

Yenisei Gulf, has very low salinity (0–2) and can be regarded as "Yenisei River water" (YR). The final water type is a small segment between the YR and OP water masses near the mouth of the Yenisei Gulf and as a large segment adjacent to the OP water mass near the Taymyr peninsula. Due to the relatively low salinity (2–12) of this water mass and its proximity to the Yenisei Gulf, we call it the "Yenisei-dominated plume water" (YP).

Once we determined the origins of the identified water masses, we extended the boundary points between the clusters located along the ship track to approximate frontal zones formed between the various water masses in region I (Figure 2) and region II (Figure 3).

3.2. Validation Against Satellite Data

The spatial structure of the Ob-Yenisei plume obtained from the cluster analysis of the in situ data collected in the surface layer requires specific quantitative and qualitative validation. We need to prove that the resulting configuration of clusters is not a statistical artifact and represents the real disposition of different water masses within the Ob-Yenisei plume. For this purpose, we validated the estimated frontal zone locations against the frontal zones visible in satellite imagery.

Due to the low spatial resolution of ocean salinity satellites, e.g., 35–50 km for SMOS [*Kerr et al*., 2001] and 100–150 km for Aquarius/SAC-D [*Le Vine et al*., 2007], we used satellite imagery of ocean color that can be applied to determine the internal structure of a large river plume [e.g., *Walker*, 1996; *Thomas and Weatherbee*, 2006]. However, the Kara Sea region is often cloudy, which greatly limits the availability of optical satellite imagery. In particular, overcast skies occurred during the in situ measurements, which hampered satellite observations of the sea surface. However, cloud conditions were much better during several days preceding the period of field survey (13–16 September 2011).

The available sequence of satellite images of the study region showed that the internal structure of the Ob-Yenisei plume, particularly the location of the frontal zones in region II, were stable during 13–16 September. The direction of the net surface Ekman transport was eastward and southeastward during 13–18 September. The magnitude of the net surface Ekman transport steadily increased from 290 to 540 kg m^{-1} s^{-1} and then decreased to 370 kg m^{-1} s^{-1}. Based on these facts, we assume that the structure of the Ob-Yenisei plume did not significantly change during 13–18 September. Thus, we will use the satellite imagery acquired on 14 September, which had the best quality (i.e., the minimal cloud cover) among the available satellite data, to validate the structure of the Ob-Yenisei plume retrieved from the in situ measurements performed on 16–18 September.

Frontal zones identified by the satellite imagery are presented in Figure 4. First, the area with the lowest concentrations of TSM and Chl-a was in the northern part of the region and recognized as AS. This area has a sharp southern border (fz-1) that separates it from the Ob-Yenisei plume. Another distinct frontal zone can be identified near the mouth of the Yenisei Gulf. It appears as a narrow meandering jet, which originated along the western shore of the mouth of the Yenisei Gulf and propagated northward along the Taymyr Peninsula (fz-3). Based on the disposition of this jet and the properties of the regional water masses, we regarded this jet as a frontal zone between the Ob-dominated waters (high concentration of TSM and low concentration of Chl-a) and the Yenisei-dominated waters (low concentration of TSM and high concentration of Chl-a) [*Gordeev et al*., 1996; *Köhler et al*., 2003; *Gebhardt et al*., 2004; *Unger et al*., 2005].

Two less distinct frontal zones also can be recognized in the satellite images. One, fz-2, separates the area between fz-1 and fz-3 and represents the transition from less turbid and less fluorescent waters in the northern part of this area to greater concentrations of TSM and Chl-a in the southern part. Thus, we regard the southern part as OP, while the northern part is the OP/AS mixing zone. Another frontal zone (fz-4) is situated inside the Yenisei Gulf and separates the YP-waters with low concentrations of TSM and Chl-a at the northern part of the Yenisei Gulf from the YR-waters with high concentrations of TSM and Chl-a in the southern part. Thus, there is qualitative agreement between the general patterns and configurations of the frontal zones identified in the satellite images using the cluster analysis results (Figure 5).

3.3. Validation Against Vertical Profiling Data

To perform a quantitative validation of the clustering results, we analyzed the in situ data obtained from continuous CTD and ADCP vertical profiling measurements along the Yenisei section (Figure 6). The vertical thermohaline structure interpolated along the Yenisei section from a depth of 1–2 m to the sea bottom is presented in Figure 7. We estimated eight major constituents of the barotropic tide (M2, S2, N2, K2, K1, O1,

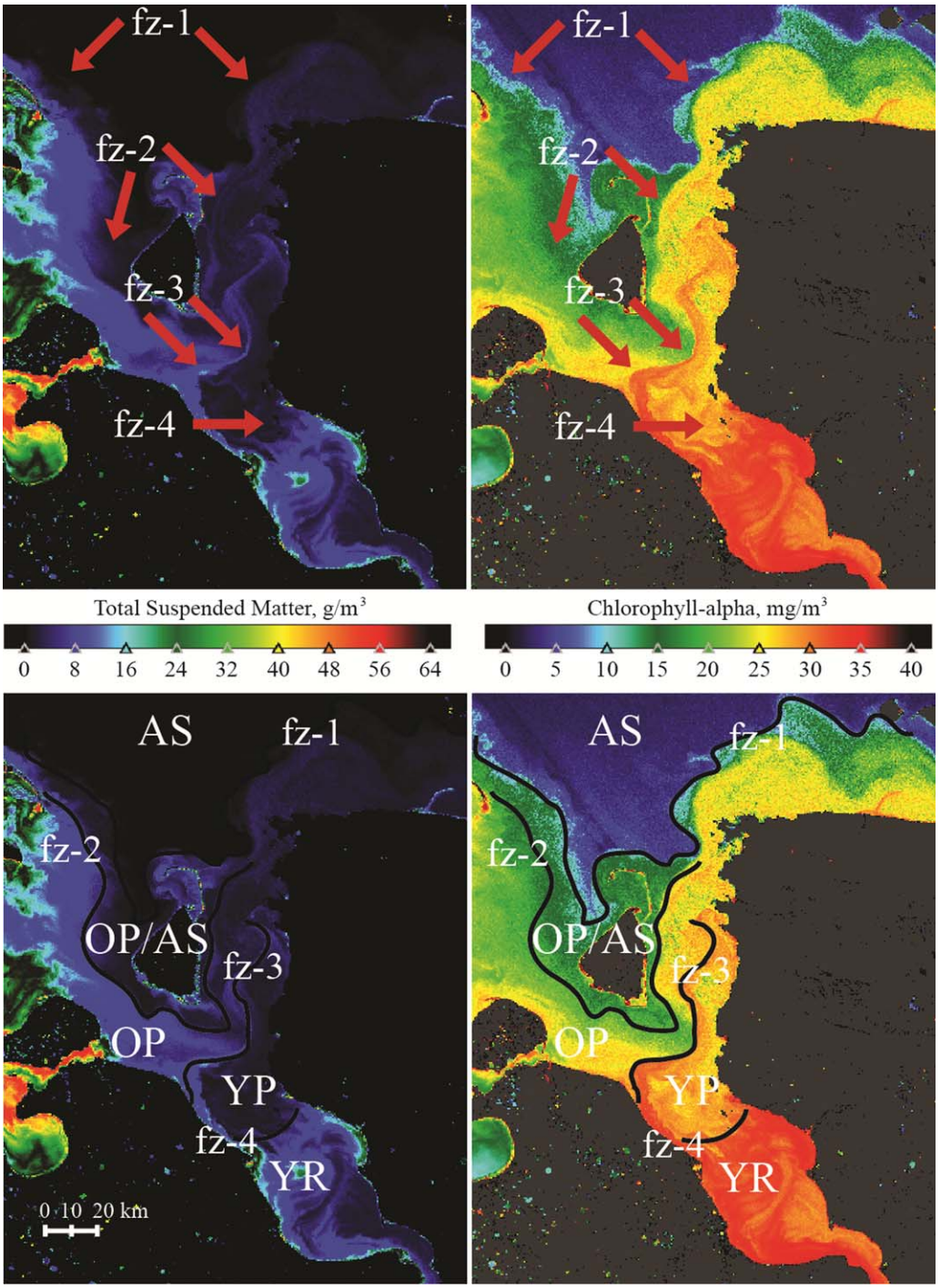

Figure 4. Frontal zones (top) and disposition of the water masses at region II according to satellite surface distributions of total suspended matter (left) and chlorophyll-α (right), on 14 September 2011.

P1, and Q1) along the Yenisei transect from the Arctic Ocean Tidal Inverse Model (AOTIM-5) [*Padman and Erofeeva*, 2004] and subtracted this estimate from the velocity data. The area to the west of the Taymyr Peninsula, where the Yenisei section is located, has a relatively flat bottom, whose depth varies mainly between 10 and 25 m (Figure 1). Therefore, baroclinic tides are not strong there and were neglected. Figure 8 illus- illustrates the resulting distribution of detided velocities from a depth of 5 m to bottom along the Yenisei section. The horizontal axis in Figures 7 and 8 represents the distance from the end of the Yenisei section located in the south.

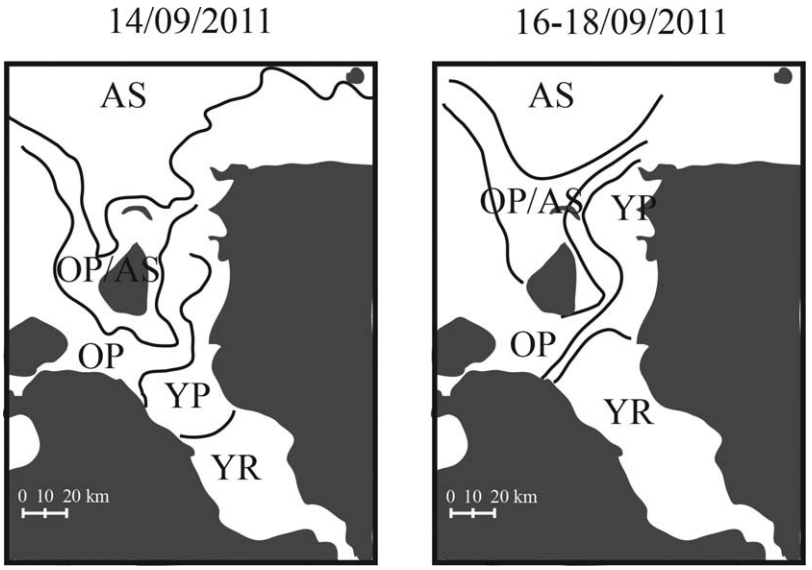

Figure 5. Configuration of the water masses of the Ob-Yenisei plume at region II obtained from satellite imagery (left) and configuration of the water types obtained from the statistical analysis (right).

Salinity ranges of different water masses identified by the clustering analysis at the surface layer have little overlaps. Transitions between YR, YP, OP, OP/AS, and AS water masses along the ship track generally correspond to salinity values equal to 2, 12, 19, and 27, respectively. Based on this fact, we regard the 2, 12, 19, and 27 isohalines obtained along the Yenisei section (and indicated in Figure 7) as the frontal zones between the different water masses of the study region. These isohalines are also shown in Figure 8 to highlight dynamical features of the different water masses along the Yenisei section.

The low salinity (0–2), warm (8–10°C) YR water mass is located in the southern part of the Yenisei section within the Yenisei Gulf. The well-mixed YR layer occupies the whole water column from the surface to the bottom as far offshore as the 10 m isobath. After YR separates from the bottom, a two-layer vertical structure is formed with sharp vertical temperature and salinity gradients below the YR water mass. YR surface salinity and temperature remain nearly constant until its northernmost extent, although bottom salinity (temperature) increases (decreases) to 28–29 (1–2°C). Approximately 30 km from the beginning of the Yenisei transect YR transforms to the 5 m deep YP water mass. Salinity (temperature) of the surface layer within the 10 km long YP water mass (30–40 km of the transect) continues to (increase) decrease to 12 (7°C). All water masses along 0–40 km of the Yenisei transect from a depth of 5 m to the bottom flow in the eastward and southeastward directions. However, the velocities of YP and YR water masses (15–20 cm/s) are significantly smaller than velocities of OP and OP/AS water masses (30–40 cm/s), which occupy the 4–10 m deep layer below them.

The surface layer (5–8 m deep) along 40–55 km of the Yenisei transect are formed by the OP and OP/AS water masses. Surface salinity (temperature) steadily increases (decreases); the highest (lowest) value is about 23 (5°C) at a distance of 50 km from the beginning of the Yenisei transect. Circulation over this portion of the Yenisei section between 5 m and the bottom was dominated by moderate (0–10 cm/s) southeastward currents. However, over 55–70 km of the Yenisei transect, the thermohaline and circulation structures change dramatically. The surface layer salinity (temperature) slowly decreases (increases) as OP/AS transforms to OP, and currents become northeastward and intensify (10–20 cm/s).

Seventy to one-hundred and five kilometers of the Yenisei transect consisted of intense northward and northwestward flow of the YP water mass (20–50 cm/s), which occupied the upper 9 m of the surface layer. Minimal (maximal) values of salinity (temperature) at the surface were 5 (7°C) at the distances of 90 and 105 km from the beginning of the Yenisei transect. The two-layered vertical structure with sharp vertical gradients (from 12 to 28 and from 6 to 2°C in the 2–4 m of water column) was observed at 85–90 km of the Yenisei transect below the YP water mass. At 95–105 km of the Yenisei transect, a wide layer (10–15 m) of

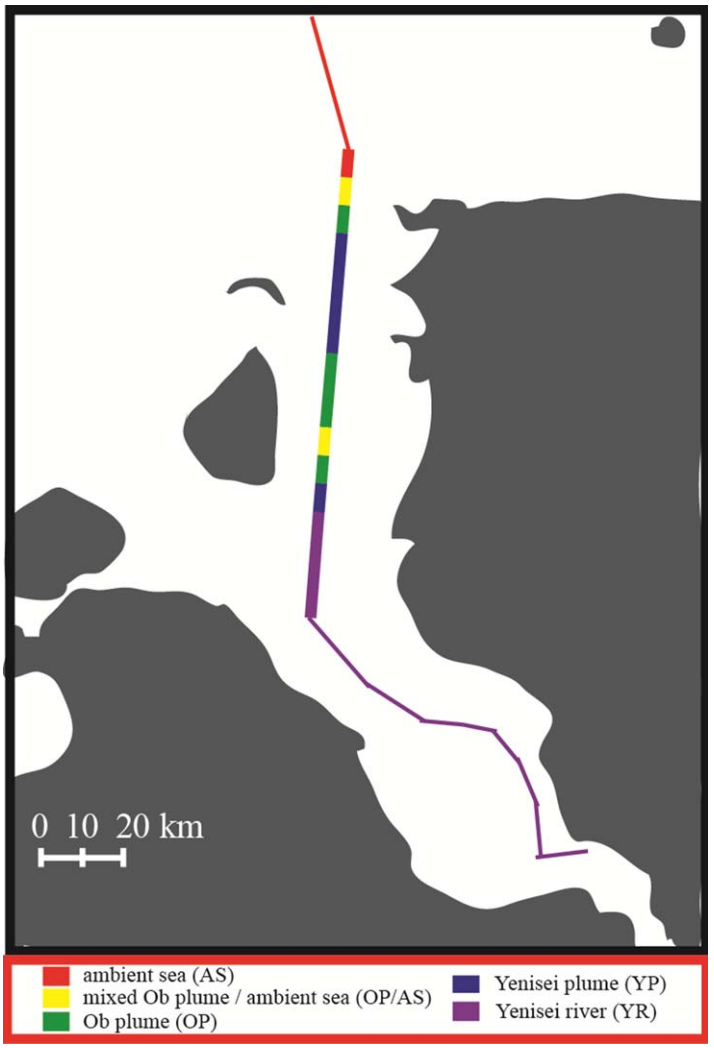

Figure 6. Disposition of different water masses along the survey track and location of the Yenisei section (solid line), along which continuous CTD and ADCP vertical profiling measurements were performed.

OP and OP/AS water masses was formed below YP, which resulted in a three-layer vertical structure (YP; OP and OP/AS; AS).

The northern part of the Yenisei transect (125–140 km) was characterized by a steady increase (decrease) of salinity (temperature) in the surface layer to 27–29 (3–4°C). Strong northeastward and southwestward flows (20–50 cm/s) of OP/AS water mass were observed to the north in the surface layer and below the northern part of the YP water mass, respectively.

4. Discussion

4.1. "Isolation" Configuration of the Ob-Yenisei River Plume

Satellite imagery and vertical profile data used for the validation of the clustering results reveal a general scheme for the formation of the structure of the Ob-Yenisei river plume. The Ob discharge formed the OP water mass that was spread over a wide area between the Gulf of Ob and the Taymyr Peninsula as a result of strong eastward and southeastward Ekman transport, as addressed in section 3.3. Mixing of OP with ambient sea resulted in the formation of the OP/AS water mass. The Yenisei discharge formed the YP water mass that propagated northward along the Taymyr Peninsula as a narrow coastal current in response to northward and northeastward wind forcing.

Indeed, the vertical profile measurements revealed eastward flow (10–20 cm s^{-1}) of the YR and YP water masses near the mouth of the Yenisei Gulf, where the narrow coastal current is formed. On the other hand, the intense eastward flow of OP and OP/AS water masses below the less dense YP waters was registered by ADCP measurements near the Yenisei Gulf and at the northern part of the Yenisei transect (Figure 8). Based on the obtained surface distribution of water masses and wind reanalysis, we presume that this flow was caused by downwelling of more saline OP and OP/AS below YP. As a result, YP was isolated from AS by OP and OP/AS water masses, which reduced salinity gradients and, thus, caused slow increase of salinity of YP. Deep (5–8 m) and strong (20–50 cm/s) alongshore jet of the low-saline (5–8) YP waters was registered approximately 100 km far from the Yenisei Gulf. A well-developed three-layer vertical structure (YP; OP and OP/AS; AS) with steep salinity gradient in this region was presumably caused by the OP and OP/AS downwelling flow as shown in Figure 7.

To validate and clarify the dynamical interpretation of the formation of the Ob-Yenisei plume configuration (hereinafter, the "isolation" configuration), we analyzed MERIS/EnviSat satellite images of the study region taken in 2005–2011 during July–October when the southern part of the Kara Sea was free of ice. Due to a

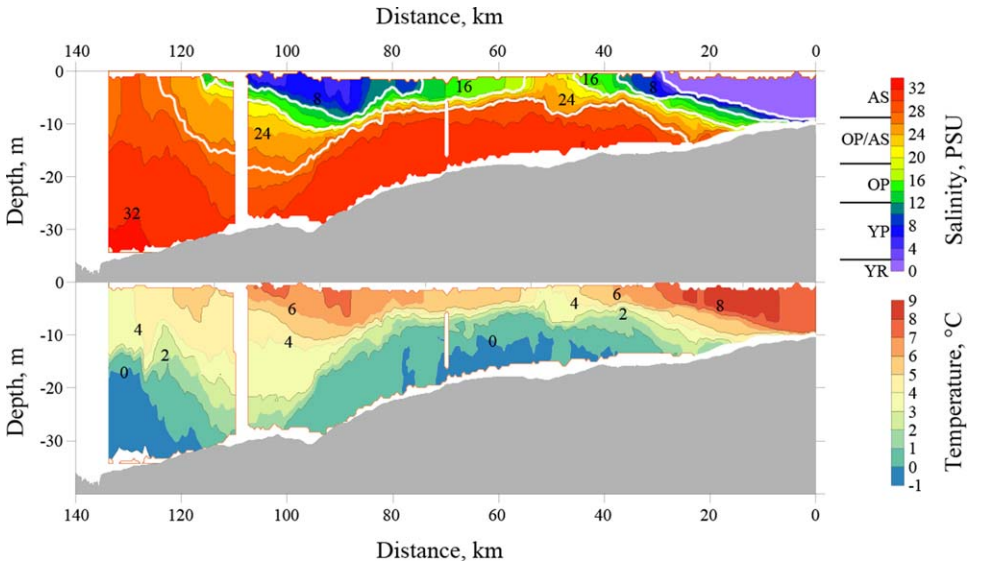

Figure 7. The vertical thermohaline structure along the Yenisei section: salinity (top) and temperature (bottom). White contours at the top represent frontal zones between different water masses, namely, 2, 12, 19, and 27.

common overcast weather, we detected only 19 periods (1–5 days long) when the area adjacent to the Ob and Yenisei gulfs was free of clouds and the configuration of the Ob-Yenisei plume could be identified.

The "isolation" configuration of the Ob-Yenisei plume was distinctly observed only in 6 cases of the 19 considered periods (Table 1). The other 13 cases were characterized by the opposite pattern of the Ob-Yenisei plume (hereinafter, "nonisolation" configuration).

A typical example of the "nonisolation" configuration was observed on 1 August 2008 (Figure 9). The Ob-dominated water mass, characterized by elevated concentrations of TSM and Chl-a, was located in the western part of the study region and had a sharp border (fz-1) with ambient sea water, identified by the lowest concentrations of TSM and Chl-a. The Yenisei-dominated water mass (YP) occupied about half of the area between the Taymyr Peninsula and the Gulf of Ob and was separated by a frontal zone (fz-3) from the more

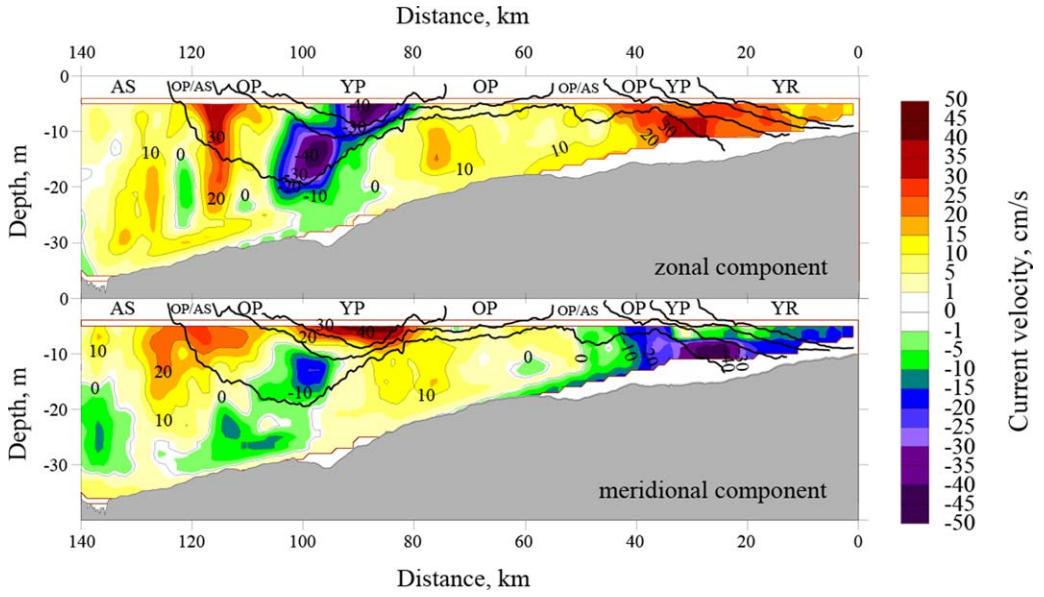

Figure 8. The vertical structure of currents along the Yenisei section: zonal (directed eastward, top) and meridional (directed northward, bottom) components of current velocities. Black lines indicate frontal zones between different water masses, obtained from salinity measurements.

Table 1. Configurations of the Ob-Yenisei Plume, Wind Forcing Conditions, and Discharges of the Yenisei and Ob Rivers During the Selected Periods in 2005–2011

Date	Presence of the "Isolation" Configuration	Averaged Zonal Wind Stress, $\times 10^3$ N/m^2	Averaged Meridional Wind Stress, $\times 10^3$ N/m^2	Yenisei Discharge, $\times 10^3$ m^3/s	Ob Discharge, $\times 10^3$ m^3/s
10 Jul 2005	–	−31.6	−22.8	90	5
1 Sep 2005	+	6.9	21.6	18	35
20 Jul 2006	–	9.2	51.0	70	5
3 Aug 2006	–	−24.4	−30.1	30	5
30 Aug 2006	+	3.6	18.0	20	35
5 Jul 2007	–	−17.9	−14.7	95	5
1 Aug 2007	–	−28.8	−15.5	40	10
16 Sep 2007	+	−7.4	21.1	20	38
3 Jul 2008	–	−21.7	−43.9	110	5
24 Jul 2008	–	−7.8	27.6	50	6
1 Aug 2008	–	−6.0	−3.4	40	7
24 Aug 2008	+	−23.0	47.6	22	38
7 Sep 2008	+	−12.0	95.4	24	35
17 Aug 2009	–	10.2	36.3	20	20
30 Jul 2010	–	35.4	−16.2	40	10
18 Aug 2010	–	8.6	46.9	20	35
15 Jul 2011	–	5.4	−13.5	30	8
8 Aug 2011	–	4.9	10.5	20	38
12 Sep 2011	+	18.2	26.0	20	28

turbid Ob-dominated water mass. The zonal width of YP increased from 60 km near the mouth of the Yenisei Gulf to 100 km at the northern part of the study region, where the frontal zones separated YP from ambient sea water (fz-2) and the turbid waters of the buoyant plume formed by the discharge of the Pyasina River (fz-4).

4.2. Wind Forcing and River Discharge Conditions

River discharge rates and local wind forcing are the main factors that govern plume structure and its dynamical characteristics [e.g., *Whitney and Garvine*, 2005; *Horner-Devine et al*., 2015].The discharge rates of Ob and Yenisei rivers and estimates of the Ekman transport averaged over the study area (72.5°N–74°N, 72.5°E–81°E) and over a period of 3 days preceding satellite measurements (described in section 2) for the 19 selected periods, along with the indication of the occurrence of the "isolation" configuration, are shown in Figure 10.

Based on the disposition of the frontal zones visible in the satellite imagery, we estimated surface areas occupied by the YP water mass for all considered periods. Figure 11 illustrates dependence of the area of the Yenisei-dominated part of the plume on the zonal (M_x) and meridional (M_y) Ekman transport as well as

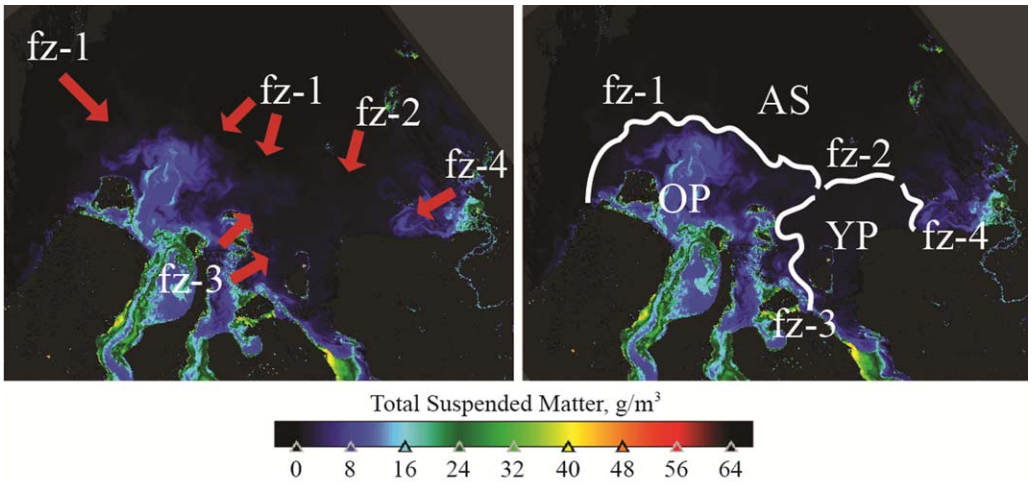

Figure 9. Frontal zones (left) and disposition of the water masses at the study region according to satellite surface distribution of total suspended matter (right) illustrating the "nonisolation" configuration of the Ob-Yenisei plume observed on 1 August 2008.

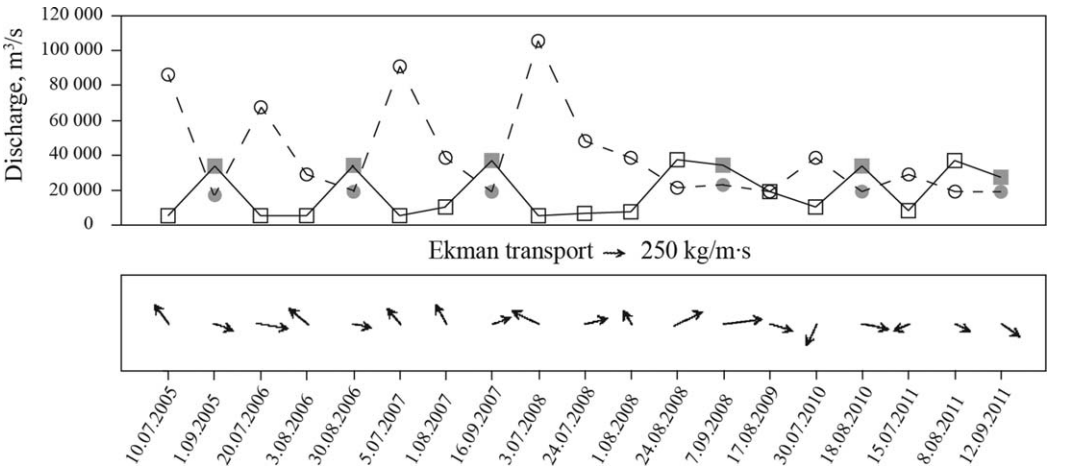

Figure 10. Discharges of the Yenisei (circles and dashed lines) and Ob (squares and solid lines) rivers (top) and Ekman transport (bottom) for the "isolation" (filled circles/squares) and "nonisolation" (empty circles/squares) periods observed by satellite imagery during 2005–2011.

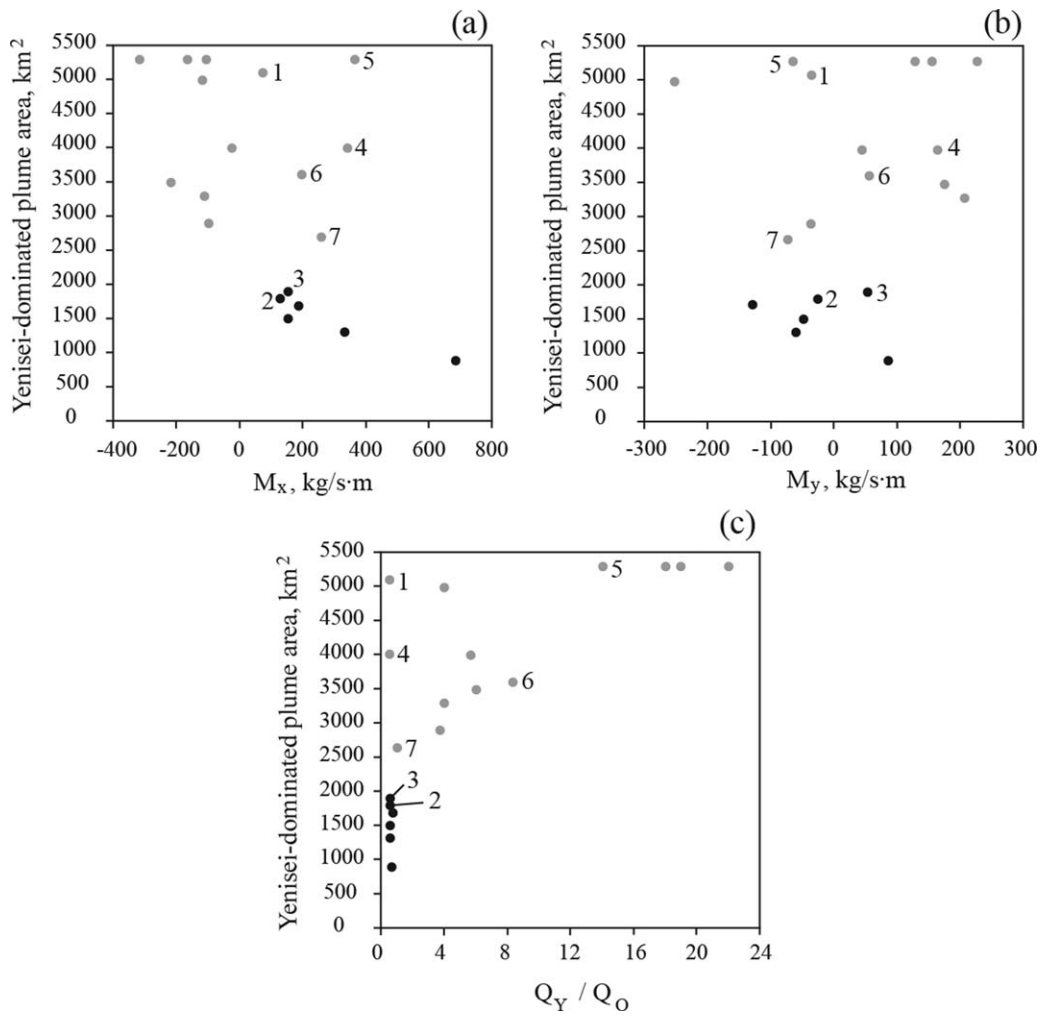

Figure 11. Dependence of the area of the Yenisei-dominated part of the plume on the zonal (a) and the meridional (b) components of Ekman transport and the ratio of discharges of the Yenisei and Ob rivers (c) for the "isolation" (black) and "nonisolation" (gray) periods observed at the satellite imagery during 2005–2011. The following cases referred in the text were indicated by the following numbers: 8 August 2011 (1), 30 August 2006 (2), 16 September 2007 (3), 24 August 2008 (4), 20 July 2006 (5), 24 July 2008 (6), 17 August 2009 (7).

on the ratio of the discharges of the Yenisei and Ob rivers with an indication of the occurrence of the "isolation" configuration.

Figures 10 and 11 show that all considered "isolation" configuration periods were preceded by strong northward winds, which induced eastward Ekman transport with M_x equal to 130–680 kg m^{-1} s^{-1}. Figure 11 reveals a negative correlation between the surface area occupied by the YP water mass and zonal Ekman transport during the "isolation" periods. Moreover, it appears that if the zonal Ekman transport was small (<100 kg m^{-1} s^{-1}) the "isolation" configuration did not form. For example, all external forcing parameters were similar on 8 August 2011 ("nonisolation" configuration) and 30 August 2006 ("isolation" configuration), except M_x, which was equal to 75 kg m^{-1} s^{-1} on 8 August 2011 and 130 kg m^{-1} s^{-1} on 30 August 2006.

Second, the magnitudes of the meridional components of Ekman transport for the "isolation" periods were relatively small and varied between −130 and 90 kg m^{-1} s^{-1}. Moreover, a large value of M_y was a negative factor for the formation of the "isolation" configuration, which can be shown by comparing the external forcing conditions observed on 16 September 2007 ("isolation" configuration) and 24 August 2008 ("nonisolation" configuration). The Ob and Yenisei discharge rates were almost equal during both periods. Although the value of M_x on 24 August 2008 (340 kg m^{-1} s^{-1}) was twice than of 16 September 2007 (150 kg m^{-1} s^{-1}), the large value of M_y (170 kg m^{-1} s^{-1}) on 24 August 2008 compared to 50 kg m^{-1} s^{-1} on 16 September 2007 caused significant northward propagation of the OP water mass and hindered the isolation of the YP water mass between the Gulf of Ob and the Taymyr Peninsula.

River discharge rates also play a crucial role in the formation of the "isolation" configuration. The Ob discharge exceeded the Yenisei discharge during all "isolation" events; otherwise, the "isolation" configuration did not form even if wind forcing conditions were "isolation" favorable. This situation was observed on 20 July 2006 and 24 July 2008 when the YP water mass formed under Yenisei discharges of 50,000 and 70,000 m^3 s^{-1}, respectively, and occupied a very large area. The Yenisei water mass was not isolated by the Ob-dominated waters even though northward winds were strong, $M_x = 370$ and 200 kg m^{-1} s^{-1}, $M_y = -70$ and 60 kg m^{-1} s^{-1} on 20 July 2006 and 24 July 2008, respectively. Finally, if both Ob and Yenisei discharges were as low as observed on 17 August 2009 (when both discharged at 20,000 m^3 s^{-1}), the area of the OP water mass is too small to isolate the Yenisei-dominated waters.

4.3. Dynamical Interpretation

We suggest the following dynamical interpretation of the formation of the "isolation" configuration. First, northward winds, on the one hand, induce downwelling flow along the Taymyr Peninsula, which causes the formation of a deep and narrow jet of YP and, on the other hand, cause the eastward Ekman transport of OP water mass. The latter process can induce downwelling of moderate salinity Ob-dominated waters under low-salinity Yenisei-dominated waters and cause formation of a three-layered vertical structure along the Taymyr Peninsula.

As shown by *Cenedese et al.* [2012] the transition from two-layered to three-layered vertical structures causes decrease in the baroclinic pressure gradient at the western front of the YP water mass from $-g'_{31}\frac{\partial h_1}{\partial x}$ to $-g'_{31}\frac{\partial h_1}{\partial x}-g'_{32}\frac{\partial h_2}{\partial x}$, where $g'_{ij}=g\frac{\rho_i-\rho_j}{\rho_0}$ is the reduced gravity, ρ_0 is the reference density, ρ_i is the density of fluid i, g is the gravitational acceleration, h_i is the thickness of fluid i, YP, OP, and AS correspond to fluids 1, 2, and 3, respectively. Thus, this mechanism induces eastward shear of the western front of the YP water mass, which narrows and intensifies the flow of the Yenisei-dominated plume.

The extent of isolation of the YP water mass from the underlying ambient sea water by Ob-dominated waters and, therefore, the salinity of YP depends on the vertical overlap of YP and OP. According to *Cenedese et al.* [2012], if two buoyant fluids with different densities are in geostrophic equilibrium in a more dense ambient fluid, their horizontal and vertical alignments are determined by the ratio of baroclinic Rossby radii of deformation $\Gamma_1 = \lambda_{31}/\lambda_{21}$ and $\Gamma_2 = \lambda_{32}/\lambda_{21}$, where $\lambda_{ij}=\sqrt{g'_{ij}H_j}\Big/f$ is the baroclinic Rossby radius of deformation between fluids i and j, H_i is the initial depth of fluid i, f is the Coriolis parameter.

Based on the vertical profiling data obtained in the mid-September 2011 (Figure 7) we prescribe densities of the Yenisei-dominated waters (ρ_1), Ob-dominated waters (ρ_2), and ambient sea (ρ_3) as equal to 1005, 1016, and 1030 kg m^{-3}, respectively, and depths of the Yenisei-dominated (H_1) and Ob-dominated (H_2) water masses as equal to 7 and 5 m, respectively. In this configuration, we have $g'_{31}/g'_{21} = 2.27$,

$g'_{32}/g'_{21} = 1.27$, so the ratios of baroclinic Rossby radii of deformation are the following: $\Gamma_1 = \lambda_{31}/\lambda_{21} = \sqrt{g'_{31}H_1}/\sqrt{g'_{21}H_1} = 1.51$, $\Gamma_2 = \lambda_{32}/\lambda_{21} = \sqrt{g'_{32}H_2}/\sqrt{g'_{21}H_1} = 0.96$.

The obtained values of Γ_1 and Γ_2 indicate that the YP and OP water masses are vertically aligned, i.e., a significant part of the western front of YP is isolated by OP from mixing with ambient sea water. Dependence of horizontal and vertical alignments of two buoyant fluids on Γ_1 and Γ_2 values was derived by *Cenedese et al*. [2012] under the assumption of geostrophic equilibrium, in particular, in the absence of wind forcing. Nevertheless, northward winds that cause the formation of a three-layered structure will intensify downwelling flow of Ob waters below Yenisei waters and, thus, wind forcing will tend to increase their vertical overlapping and isolation of the YP water mass.

4.4. Seasonal and Interannual Variability

In order to estimate the frequency and duration of the occurrence of the assumed "isolation" configuration of the Ob-Yenisei plume, we parameterized its formation conditions by the following inequalities: $M_x > 100$ kg m^{-1} s^{-1}, $M_y < 100$ kg m^{-1} s^{-1}, $Q_O > 20{,}000$ m^3 s^{-1}, and $Q_Y/Q_O < 1$, where Q_O and Q_Y are the Ob and Yenisei discharge rates, respectively. Then, by applying these inequalities to ERA-Interim wind reanalysis and river discharge data, we identified 36 periods of "isolation"-favorable conditions during the ice-free seasons of 2005–2011 (Figure 12).

The duration of the majority of the identified "isolation"-favorable periods varied between 1 and 8 days, while their total duration was equal to 133 days, which is only 19 days per year on the average. However, the "isolation"-favorable conditions occurred only during late summer and autumn when, first, the atmospheric circulation at the southeastern part of the Kara Sea is dominated by northward winds, second, the Ob discharge exceeded the Yenisei discharge, and, third, the southern part of the Kara Sea is free of ice. The average duration of the "isolation" periods in August, September, and October was equal to 4, 8, and 7 days, respectively.

The number of "isolation" days showed substantial interannual variability from 11 in 2011 to 29 in 2009, caused mainly by the interannual variability of local atmospheric circulation. As a result, the total duration of the "isolation" periods, which is negligible on an annual scale, is much more significant during certain weeks and months. In particular, the Yenisei-dominated part of the plume was estimated to be isolated from the sea water during approximately 50% of days during September–October 2009, including 18 successive days from 27 September till 14 October 2009. Moreover, 8 of 14 considered Septembers and Octobers were characterized by at least 8 "isolation" days.

5. Conclusions

A large set of in situ data was collected in the southern part of the Kara Sea influenced by the Ob and Yenisei river discharge in September 2011. Based on the statistical analysis of these data, we identified a complex spatial structure of the buoyant plume formed by the Ob and Yenisei runoff and distinguished the Ob- and Yenisei-dominated water masses, characterized by different physical, chemical, and dynamical properties. These results were validated using satellite imagery and vertical CTD and ADCP profiling data.

We showed that in mid-September 2011, the Ob-dominated water mass was spread over more than 25,000 km^2 between the Gulf of Ob and the Taymyr Peninsula as a result of eastward Ekman transport and that plume properties were significantly modified by mixing with ambient sea water. On the other hand, the Yenisei-dominated water mass formed a narrow coastal current and propagated northward from the Yenisei Gulf along the Taymyr Peninsula. The Yenisei-dominated water mass was isolated from ambient sea water by the Ob-dominated water mass. As a result, the salinity of the Yenisei-dominated water was significantly lower than of the Ob-dominated waters, while its area was less than 2000 km^2.

In particular, the 35 km long and 5–9 m deep surface layer of the Yenisei-dominated water mass, with a salinity of ~5–8, was observed ~100 km to the north from the Yenisei Gulf. Such low salinity values far from the freshwater source are typical for long river estuaries and the near-field part of the large Amazon river plume [*Lentz and Limeburner*, 1995; *Geyer et al*., 1996]. However, to the best of our knowledge, such salinity values were not registered at far-field parts of buoyant plumes located in the open sea, including those formed by the world's largest rivers such as the Congo [*Eisma and Van Bennekom*, 1978; *Denamiel et al*., 2013],

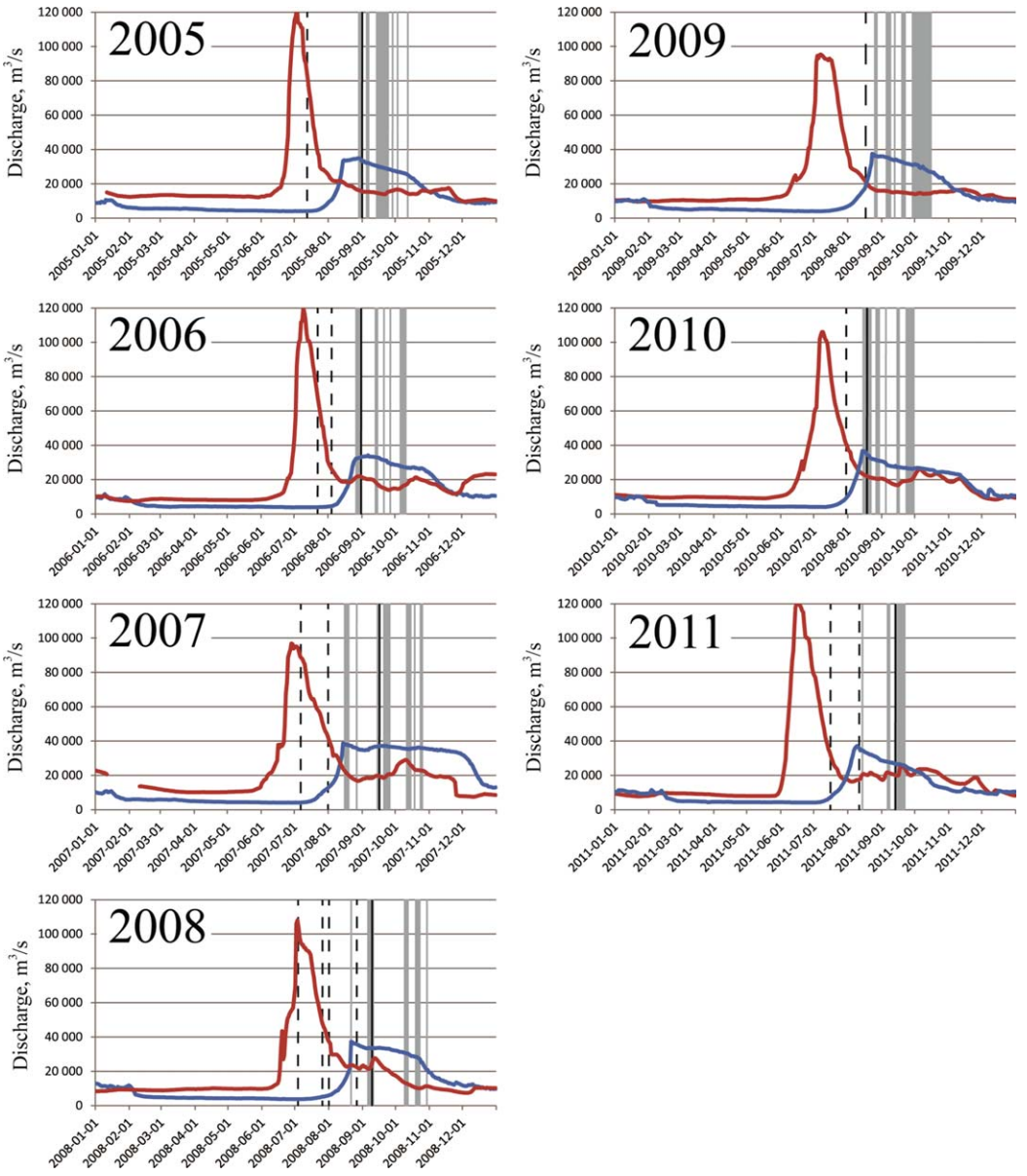

Figure 12. Discharges of Ob (blue lines) and Yenisei (red lines) into the Kara Sea in 2005–2011 and periods of the "isolation"-favorable conditions (gray bands) identified using ERA-Interim wind reanalysis. The "isolation" (solid lines) and "nonisolation" (dashed lines) configurations of the Ob-Yenisei plume observed at the satellite imagery are indicated.

Yangtze [*Beardsley et al*., 1985; *Yuan et al*., 2016], Orinoco [*Bonilla et al*., 1993; *Del Castillo et al*., 1999], and Mississippi [*Schiller et al*., 2011; *Huang et al*., 2015] rivers.

Based on satellite imagery, the ERA-Interim wind reanalysis, and gauge measurements of the Yenisei and Ob discharge, we suggest that the formation of the "isolation" configuration is induced by high discharge of the Ob River, low discharge of the Yenisei River, and strong northward wind forcing. These external forcing conditions cause eastward Ekman transport and downwelling of more dense Ob-dominated waters below the Yenisei-dominated waters along the Taymyr Peninsula and result in a vertical alignment of these water masses. However, the response of a stratified inner shelf to cross-shelf wind forcing, in particular, its role in driving along-shelf flows, has received little attention yet and is not extensively studied, especially in areas with complex bathymetry and shoreline [*Lentz and Fewings*, 2012]. Thus, the dynamical interpretation described above requires verification based on more specific and detailed in situ measurements in the

study region and/or numerical modeling of interaction between the Ob and Yenisei plumes under various external forcing conditions.

We identified periods of potential formation of the "isolation" configuration during 2005–2011. The monthly average duration of the "isolation"-favorable conditions was equal to 4 days in August, 8 days in September, and 7 days in October. The majority of the potential "isolation" events lasted from 1 to 8 days, and their average duration was 4 days. However, the total annual duration of the "isolation"-favorable conditions as well as their monthly distribution showed significant interannual variability. The most frequent and long-term "isolation" events occurred in September–October 2009, when the Yenisei-dominated water mass was isolated from the ambient sea during 29 days, including 18 successive days from 27 September to 14 October 2009.

The formation of the "isolation"/"nonisolation" configuration determines areas occupied by Ob- and Yenisei-dominated waters with significantly different water properties. Long-term and/or frequent occurrence of the "isolation" configuration of the Ob-Yenisei plume can cause increased absorption of solar radiation by turbid Ob-dominated surface waters over the large area between the Gulf of Ob and the Taymyr Peninsula compared to the "nonisolation" configuration. Also, it could result in the northward transport of a large volume of low-saline Yenisei-dominated water to the open part of the Kara Sea. This transport is presumed to occur mainly in September–October, when the "isolation"-favorable wind and discharge conditions are typical in the study region. As a result, it can decrease the salinity of the surface water and, thus, accelerate ice formation in the central part of the Kara Sea, which starts in late October as was revealed for the other Arctic seas [*Bauch et al*., 2013; *Nghiem et al*., 2014; *Whitefield et al*., 2015]. Spreading of the low-saline Yenisei-dominated water along the Taymyr Peninsula can modify distributions of river, brackish, and marine plankton communities and, therefore, influence primary productivity and local food webs.

Interaction and collision of two or multiple river plumes and formation of a joint buoyant plume is a common process for coastal areas, e.g., with closely spaced river mouths [*Warrick and Farnsworth*, 2017; *Osadchiev and Korshenko*, 2017] and/or with large buoyant plumes, which occupy long segments of sea shore [*Burrage et al*., 2008]. These processes significantly influence spreading dynamics of river plumes, as well as local transport patterns of river-borne sediments, nutrients, and pollutants, and, therefore, govern local physical, biological, and geochemical processes. A number of previous studies focused on subduction of more dense plumes underneath more buoyant plumes, however, with idealized bathymetry and shorelines and/or in absence of wind forcing [*Marmorino et al*., 1998; *Cenedese et al*., 2012; *Warrick and Farnsworth*, 2017]. Thus, the dynamical mechanism of formation of subduction of water masses with different densities in response to wind forcing, addressed in this study, could be useful for studying the related issues in many world coastal areas.

Finally, the presented method of forecasting the spatial structure of a river plume based on river discharge and wind reanalysis data, which can be adapted and adjusted using both in situ and satellite measurements, hold promise of providing improved qualitative and quantitative insights into river plume dynamics and related coastal processes, especially for poorly sampled areas.

Acknowledgments

The authors are grateful to many colleagues at Shirshov Oceanology Institute for their valuable support during the fieldwork and the provided in situ data. The article benefited from critical comments and constructive suggestions from Thomas Weingartner and anonymous reviewers. This research was funded by the Russian Scientific Foundation [grant 14–50-00095]. The MERIS/Envisat satellite data were downloaded from the European Space Agency (ESA) repository of the Envisat satellite data http://merisfrs-merci-ds.eo.esa.int/merci (available after registration). The river discharge data were downloaded from the Arctic Great Rivers Observatory (Arctic GRO) website http://arcticgreatrivers.org/data.html (available after registration). The ERA-Interim reanalysis data were downloaded from the European Centre for Medium-Range Weather Forecasts (ECMWF) website http://apps.ecmwf.int/datasets/. The Arctic Ocean Tidal Inverse Model data is available at https://www.esr.org/polar_tide_models/Model_AOTIM5.html/. The in situ data used in this paper are available on request from the authors.

References

Bauch, D., J. A. Hölemann, A. Nikulina, C. Wegner, M. A. Janout, L. A. Timokhov, and H. Kassens (2013), Correlation of river water and local sea-ice melting on the Laptev Sea shelf (Siberian Arctic), *J. Geophys. Res. Oceans*, *118*, 550–561, doi:10.1002/jgrc.20076.

Beardsley, R. C., R. Limeburner, H. Yu, and G. A. Cannon (1985), Discharge of the Changjiang (Yangtze river) into the East China sea, *Cont. Shelf Res.*, *4*, 57–76, doi:10.1016/0278-4343(85)90022-6.

Bonilla, J., W. Senior, J. Jugden, O. Zafiriou, and R. Jones (1993), Seasonal distribution of nutrients and primary productivity on the eastern continental shelf of Venezuela as influenced by the Orinoco River, *J. Geophys. Res.*, *98*(C2), 2245–2257, doi:10.1029/92JC02761.

Burrage, D., J. Wesson, C. Martinez, T. Pérez, O. Möller, and A. Piola (2008), Patos Lagoon outflow within the Río de la Plata plume using an airborne salinity mapper: Observing an embedded plume, *Cont. Shelf Res.*, *28*, 1625–1638, doi:10.1016/j.csr.2007.02.014.

Carmack, E. C., et al. (2016), Freshwater and its role in the Arctic Marine System: Sources, disposition, storage, export, and physical and biogeochemical consequences in the Arctic and global oceans, *J. Geophys. Res. Biogeosci.*, *121*, 675–717, doi:10.1002/2015JG003140.

Cenedese, C., J. A. Lerczak, and G. Bartone (2012), A geostrophic adjustment model of two buoyant fluids, *J. Phys. Oceanogr.*, *42*, 1932–1944, doi:10.1175/jpo-d-11-0169.1.

Del Castillo, C. E., P. G. Coble, J. M. Morell, J. M. Lopez, and J. E. Corredor (1999), Analysis of the optical properties of the Orinoco River plume by absorption and fluorescence spectroscopy, *Mar. Chem.*, *66*, 35–51, doi:10.1016/s0304-4203(99)00023-7.

Denamiel, C., W. P. Budgell, and R. Toumi (2013), The Congo River plume: Impact of the forcing on the far-field and near-field dynamics, *J. Geophys. Res. Oceans*, *118*, 964–989, doi:10.1002/jgrc.20062.

Dianskii, N. A., V. V. Fomin, V. M. Gruzinov, I. M. Kabatchenko, and G. I. Litvinenko (2015), Estimation of influence of the ship channel of the Sabetta Harbour on change of hydrological conditions of the Gulf of Ob using numerical modelling [in Russian], *Arctic Ecol. Econ.*, *3*, 18–29.

Dickson, A. G., J. D. Afghan, and G. C. Anderson (2003), Reference materials for oceanic CO_2 analysis: A method for the certification of total alkalinity, *Mar. Chem.*, *80*, 185–197, doi:10.1016/s0304-4203(02)00133-0.

Dmitrenko, I. A., V. A. Gribanov, D. L. Volkov, S. L. Berezovskaya, and H. Kassens (2000), The role of river runoff in the interannual variability of the fast ice extension in the Russian Arctic [in Russian], *Russ. Meteorol. Hydrol.*, *3*, 85–94.

DOE (1994), *Handbook of Methods for Analysis of the Various Parameters of the Carbon Dioxide System in Sea Water. Version 2*, edited by A. Dickson and C. Goyet, ORNL/CDIAC-74, USA, doi:10.2172/10107773.

Doerffer, R., and H. Schiller (1997), Pigment index, sediment and gelbstoff retrieval from directional water leaving radiance reflectances using inverse modelling technique—MERIS algorithm theoretical basis document 2.12, Version 4, GKSS Res. Cent., Geesthacht, Germany.

Doerffer, R., and H. Schiller (2008), MERIS regional, coastal and lake case 2 water project—Atmospheric correction ATBD, Version 1.0, GKSS Res. Cent., Geesthacht, Germany.

Dolgopolova, E. N. (2015), Regularities in the motion of water and sediments at the mouth of a river of estuarine-deltaic type: Case study of the Yenisei River, *Water Resour.*, *42*, 198–207, doi:10.1134/s0097807815020050.

Dubinina, E. O., S. A. Kossova, A. Y. Miroshnikov, and R. V. Fyaizullina (2017), Isotope parameters (δD, δ^{18}O) and sources of freshwater input to Kara Sea, *Oceanology*, *57*, 31–40, doi:10.1134/S0001437017010040.

Eisma, D., and A. J. Van Bennekom (1978), Zaire River and estuary and the Zaire outflow in the Atlantic Ocean, *Netherlands J. Sea Res.*, *12*, 255–272, doi:10.1016/0077-7579(78)90030-3.

Edmond, J. M. (1970), High precision determination of titration alkalinity and total carbon dioxide content of sea water by potentiometric titration, *Deep Sea Res. Oceanogr. Abstr.*, *17*, 737–750, doi:10.1016/0011-7471(70)90038-0.

Fomferra, N., and C. Brockmann (2015), The BEAM project web page, Carsten Brockmann Consult, Hamburg, Germany. [Available at http://www.brockmann-consult.de/cms/web/beam/.]

Galimov, E. M., L. A. Kodina, O. V. Stepanets, and G. S. Korobeinik (2006), Biogeochemistry of the Russian Arctic. Kara Sea: Research results under the SIRRO project, 1995–2003, *Geochem. Int.*, *44*, 1053–1104, doi:10.1134/s0016702906110012.

Gebhardt, A. C., B. Gaye-Haake, D. Unger, N. Lahajnar, and V. Ittekkot (2004), Recent particulate organic carbon and total suspended matter fluxes from the Ob and Yenisei Rivers into the Kara Sea (Siberia), *Mar. Geol.*, *207*, 225–245, doi:10.1016/j.margeo.2004.03.010.

Geyer, W. R., R. C. Beardsley, S. J. Lentz, J. Candela, R. Limeburner, W. E. Johns, B. M. Castro, and I. D. Soares (1996), Physical oceanography of the Amazon shelf, *Cont. Shelf Res.*, *16*, 575–616, doi:10.1016/0278-4343(95)00051-8.

Gordeev, V. V., and V. V. Tsirkunov (1998), River fluxes of dissolved and suspended substances, in *A Water Quality Assessment of the Former Soviet Union*, edited by V. Kimstach, M. Meybeck, and E. Baroudy, pp. 310–350, E & FN Spon, London, U. K.

Gordeev, V. V., J. M. Martin, J. S. Sidorov, and M. V. Sidorova (1996), A reassessment of the Eurasian river input of water, sediment, major elements, and nutrients to the Arctic Ocean, *Am. J. Sci.*, *296*, 664–691, doi:10.2475/ajs.296.6.664.

Graevskii, A. P., E. P. Kotrekhov, A. A. Matveev, and A. V. Ufimtsev (1980), Results of studying currents in Yenisei mouth area in summer, *Trans. Arct. Antarct. Res. Inst.*, *358*, 55–74.

Harms, I. H., and M. J. Karcher (1999), Modeling the seasonal variability of circulation and hydrography in the Kara Sea, *J. Geophys. Res.*, *104*(C6), 13,431–13,448, doi:10.1029/1999JC900048.

Harms, I. H., and M. J. Karcher (2005), Kara Sea freshwater dispersion and export in the late 1990s, *J. Geophys. Res.*, *110*, C08007, doi:10.1029/2004JC002744.

Horner-Devine, A. R., R. D. Hetland, and D. G. MacDonald (2015), Mixing and transport in coastal river plumes, *Annu. Rev. Fluid Mech.*, *47*, 569–594, doi:10.1146/annurev-fluid-010313-141408.

Huang, W. J., W. J. Cai, Y. Wang, S. E. Lohrenz, and M. C. Murrell (2015), The carbon dioxide system on the Mississippi River-dominated continental shelf in the northern Gulf of Mexico: 1. Distribution and air-sea CO_2 flux, *J. Geophys. Res. Oceans*, *120*, 1429–1445, doi:10.1002/2014JC010498.

Johnson, D. R., T. A. McClimans, S. King, and T. Grenness (1997), Fresh water masses in the Kara Sea during summer, *J. Mar. Syst.*, *12*, 127–145, doi:10.1016/s0924-7963(96)00093-0.

Kagan, B. A., A. A. Timofeev, and E. V. Sofina (2010), Seasonal variability of surface and internal M2 tides in the Arctic Ocean, *Izv. Atmos. Ocean. Phys.*, *46*, 652–662, doi:10.1134/S0001433810050105.

Kagan, B. A., E. V. Sofina, and A. A. Timofeev (2011), Modeling of the M2 surface and internal tides and their seasonal variability in the Arctic Ocean: Dynamics, energetics and tidally induced diapycnal diffusion, *J. Mar. Res.*, *69*, 245–276, doi:10.1357/002224011798765312.

Kerr, Y. H., P. Waldteufel, J.-P. Wigneron, J. Martinuzzi, J. Font, and M. Berger (2001), Soil moisture retrieval from space: The Soil Moisture and Ocean Salinity (SMOS) mission, *IEEE Trans. Geosci. Remote Sens.*, *39*(8), 1729–1735, doi:10.1109/36.942551.

Köhler, H., B. Meon, V. V. Gordeev, A. Spitzy, and R. M. W. Amon (2003), Dissolved organic matter (DOM) in the estuaries of Ob and Yenisei and the adjacent Kara Sea, Russia, in *Proceedings in Marine Science*, vol. 6, pp. 281–308, Elsevier, Amsterdam.

Kubryakov, A. A., S. V. Stanichny, and A. G. Zatsepin (2016), River plume dynamics in the Kara Sea from altimetry-based Lagrangian model, satellite salinity and chlorophyll data, *Remote Sens. Environ.*, *176*, 177–187, doi:10.1016/j.rse.2016.01.020.

Lentz, S. J., and R. Limeburner (1995), The Amazon River Plume during AMASSEDS: Spatial characteristics and salinity variability, *J. Geophys. Res.*, *100*, 2355–2375, doi:10.1029/94JC01411.

Lentz, S. J., and M. R. Fewings (2012), The wind- and wave-driven inner-shelf circulation, *Annu. Res. Mar. Sci.*, *4*, 317–343, doi:10.1146/annurev-marine-120709-142745.

Le Vine, D. M., G. S. E. Lagerloef, F. R. Colomb, S. H. Yueh, and F. A. Pellerano (2007), Aquarius: An instrument to monitor sea surface salinity from space, *IEEE Trans. Geosci. Remote Sens.*, *45*, 204, doi:10.1109/tgrs.2007.8980920-2050.

MacQueen, J. B. (1967), Some methods for classification and analysis of multivariate observations, in *Proceedings of 5th Berkeley Symposium on Mathematical Statistics and Probability*, vol. 1, pp. 281–297, University of California Press, Berkeley, Calif.

Makkaveev, P. N., P. A. Stunzhas, and P. V. Khlebopashev (2010), The distinguishing of the Ob and Yenisei waters in the desalinated lenses of the Kara Sea in 1993 and 2007, *Oceanology*, *50*, 698–705, doi:10.1134/s0001437010050073.

Makkaveev, P. N., Z. G. Melnikova, A. A. Polukhin, S. V. Stepanova, P. V. Khlebopashev, and A. L. Chulcova (2015), Hydrochemical characteristics of the waters of the western part of the Kara Sea, *Oceanology*, *55*, 485–496, doi:10.1134/s0001437015040116.

Marmorino, G. O., C. Y. Shen, N. Allan, F. Askari, D. B. Trizna, C. L. Trump, and L. K. Shay (1998), An occluded coastal oceanic front, *J. Geophys. Res.*, *103*(C10), 21,587–21,600, doi:10.1029/98JC02099.

McClimans, T. A., D. R. Johnson, M. Krosshavn, S. E. King, J. Carroll, and T. Grenness (2000), Transport processes in the Kara Sea, *J. Geophys. Res.*, *105*(C6), 14,121–14,139, doi:10.1029/1999JC000012.

Meade, R. H., N. N. Bobrovitskaya, and V. I. Babkin (2000), Suspended-sediment and fresh-water discharges in the Ob and Yenisey rivers, 1960–1988, *Int. J. Earth Sci.*, *89*, 461–469, doi:10.1007/s005310000107.

Mendes, R., M. C. Sousa, D. Maite, M. Gomez-Gesteira, and J. M. Dias (2016), New insights into the Western Iberian Buoyant Plume: Interaction between the Douro and Minho River plumes under winter conditions, *Prog. Oceanogr.*, *141*, 30–43, doi:10.1016/j.pocean.2015.11.006.

Neelov, I. A., and A. V. Kouraev (1996), 3-D circulation model of the Kara Sea, *NIERSC Tech. Rep. 3*, *INTAS Proj. INTAS-93–0814*, NIERSC, St. Petersburg, Russia.

Nghiem, S. V., D. K. Hall, I. G. Rigor, P. Li, and G. Neumann (2014), Effects of Mackenzie River discharge and bathymetry on sea ice in the Beaufort Sea, *Geophys. Res. Lett.*, *41*, 873–879, doi:10.1002/2013GL058956.

Nummelin, A., M. Ilicak, C. Li, and L. H. Smedsrud (2016), Consequences of future increased Arctic runoff on Arctic Ocean stratification, circulation, and sea ice cover, *J. Geophys. Res. Oceans*, *121*, 617–637, doi:10.1002/2015JC011156.

Oki, T., and S. Kanae (2006), Global hydrological cycles and world water resources, *Science*, *313*, 1068–1072, doi:10.1126/science.1128845.

Osadchiev, A., and E. Korshenko (2017), Small river plumes off the northeastern coast of the Black Sea under average climatic and flooding discharge conditions, *Ocean Sci.*, *13*, 465–482, doi:10.5194/os-13-465-2017.

Padman, L., and S. Erofeeva (2004), A barotropic inverse tidal model for the Arctic Ocean, *Geophys. Res. Lett.*, *31*, L02303, doi:10.1029/2003GL019003.

Palmer, S. C., V. V. Pelevin, I. Goncharenko, A. W. Kovacs, A. Zlinszky, M. Presing, H. Horvath, V. Nicolas-Perea, H. Balzter, and V. R. Toth (2013), Ultraviolet fluorescence LiDAR (UFL) as a measurement tool for water quality parameters in turbid lake conditions, *Int. J. Remote Sens.*, *5*, 4405–4422, doi:10.3390/rs5094405.

Panteleev, G., A. Proshutinsky, M. Kulakov, D. A. Nechaev, and W. Maslowski (2007), Investigation of the summer Kara Sea circulation employing a variational data assimilation technique, *J. Geophys. Res.*, *112*, C04S15, doi:10.1029/2006JC003728.

Pavlov, V. K., and S. L. Pfirman (1995), Hydrographic structure and variability of the Kara Sea: Implications for pollutant distribution, *Deep Sea Res., Part II*, *42*, 1369–1390, doi:10.1016/0967-0645(95)00046-1.

Pavlova, G. Yu., P. Ya. Tishchenko, T. I. Volkova, A. Dickson, and K. Wallmann (2008), Intercalibration of Bruevich's method to determine the total alkalinity in seawater, *Oceanology*, *48*, 438–443, doi:10.1134/s0001437008030168.

Pelevin, V., A. Zlinszky, E. Khimchenko, and V. R. Toth (2017), Ground truth data on chlorophyll-a, chromophoric dissolved organic matter and suspended sediment concentrations in the upper water layer as obtained by LIF lidar at high spatial resolution, *Int. J. Remote Sens.*, *38*, 1967–1982, doi:10.1080/01431161.2016.1274446.

Ramaswamy, V., P. S. Rao, K. H. Rao, S. Thwin, N. Srinivasa Rao, and V. Raiker (2004), Tidal influence on suspended sediment distribution and dispersal in the northern Andaman Sea and Gulf of Martaban, *Mar. Geol.*, *208*, 33–42, doi:10.1016/j.margeo.2004.04.019.

Robinson, R. A. J., M. I. Bird, N. W. Oo, T. B. Hoey, M. M. Aye, D. L. Higgitt, and S. L. Win (2007), The Irrawaddy River sediment flux to the Indian Ocean: The original nineteenth-century data revisited, *J. Geol.*, *115*, 629−640, doi:10.1086/521607.

Schiller, R. V., V. H. Kourafalou, P. Hogan, and N. D. Walker (2011), The dynamics of the Mississippi River plume: Impact of topography, wind and offshore forcing on the fate of plume waters, *J. Geophys. Res.*, *116*(C6), C06029, doi:10.1029/2010JC006883.

Semizhon, T., S. Rollin, Y. Spasova, and E. Klemt (2010), Transport and distribution of artificial gamma-emitting radionuclides in the River Yenisei and its sediment, *J. Environ. Radioact.*, *101*, 385–402, doi:10.1016/j.jenvrad.2010.02.012.

Smith, S. D. (1988), Coefficients for sea surface wind stress, heat flux, and wind profiles as a function of wind speed and temperature, *J. Geophys. Res.*, *93*, 15,467–15,472, doi:10.1029/jc093ic12p15467.

Thomas, A., and R. A. Weatherbee (2006), Satellite-measured temporal variability of the Columbia River plume, *Remote Sens. Environ.*, *100*, 167–178, doi:10.1016/j.rse.2005.10.018.

Unger, D., B. Gaye-Haake, K. Neumann, A. C. Gebhardt, and V. Ittekkot (2005), Biogeochemistry of suspended and sedimentary material in the Ob and Yenisei rivers and Kara Sea: Amino acids and amino sugars, *Cont. Shelf Res.*, *25*, 437–460, doi:10.1016/j.csr.2004.09.014.

Vakulovsky, S. M. (2003), Estimation and prediction of the consequences for the environment and population of radioactive contamination of the Yenisei River by discharges of the Krasnoyarsk mining and chemical industrial complex, *Final Proj. 1404*, technical report, Int. Sci. and Technol. Cent. (ISTC), SPA-Typhoon, Obninsk, Russia.

Walker, N. D. (1996), Satellite assessment of Mississippi River plume variability: Causes and predictability, *J. Remote Sens. Environ.*, *58*, 21–35, doi:10.1016/0034-4257(95)00259-6.

Warrick, J. A., and K. L. Farnsworth (2017), Coastal river plumes: Collisions and coalescence, *Prog. Oceanogr.*, *151*, 245–260, doi:10.1016/j.pocean.2016.11.008.

Whitefield, J., P. Winsor, J. Mcclelland, and D. Menemenlis (2015), A new river discharge and river temperature climatology data set for the pan-Arctic region, *Ocean Modell.*, *88*, 1–15, doi:10.1016/j.ocemod.2014.12.012.

Whitney, M. M., and R. W. Garvine (2005), Wind influence on a coastal buoyant outflow, *J. Geophys. Res.*, *110*, C03014, doi:10.1029/2003JC002261.

Yuan, R., H. Wu, J. Zhu, and L. Li (2016), The response time of the Changjiang plume to river discharge in summer, *J. Mar. Syst.*, *154*, 82–92, doi:10.1016/j.jmarsys.2015.04.001.

Yuan, Y., M. Avener, and A. R. Horner-Devine (2011), A two-color optical method for determining layer thickness in two interacting buoyant plumes, *Exp. Fluids*, *50*(5), 1235–1245, doi:10.1007/s00348-010-0969-y.

Zatsepin, A. G., P. O. Zavialov, V. V. Kremenetskiy, S. G. Poyarkov, and D. M. Soloviev (2010), The upper desalinated layer in the Kara Sea, *Oceanology*, *50*, 657–667, doi:10.1134/s0001437010050036.

Zatsepin, A. G., V. V. Kremenetskiy, A. A. Kubryakov, S. V. Stanichny, and D. M. Soloviev (2015), Propagation and transformation of waters of the surface desalinated layer in the Kara Sea, *Oceanology*, *55*, 450–460, doi:10.1134/s0001437015040153.

Zavialov, P. O., A. S. Izhitskiy, A. A. Osadchiev, V. V. Pelevin, and A. B. Grabovskiy (2015), The structure of thermohaline and bio-optical fields in the upper layer of the Kara Sea in September 2011, *Oceanology*, *55*, 461–471, doi:10.1134/s0001437015040177.